Energy 204 (2020) 117993

Contents lists available at ScienceDirect

Energy

journal homepage: www.elsevier.com/locate/energy

Performance evaluations of an adsorption-based power and cooling cogeneration system under different operative conditions and working fluids

Yanan Zhao , Zuoqing Luo , Rui Long *, Zhichun Liu , Wei Liu

School of Energy and Power Engineering, Huazhong University of Science and Technology, Wuhan, 430074, PR China

ARTICLE INFO

Article history:
Received 21 November 2019
Received in revised form
23 May 2020
Accepted 27 May 2020
Available online 31 May 2020

Keywords:
Low-grade heat
Power generation
Refrigeration
Cogeneration
Exergy efficiency

ABSTRACT

In order to harvest low-grade waste heat below 80 °C, we present an alternative adsorption-based power and cooling cogeneration system, which consists of an adsorption-based desalination system for generating concentrated and diluted salt solutions as well as providing cooling power, and a pressure retarded osmosis system for converting the produced salinity gradient energy into electricity. Effects of operation conditions, adsorbents, salt types and solvents are systematically investigated to evaluate the coefficient of performance (COP), electric efficiency, and exergy efficiency of the hybrid system. Results reveal that there exists an optimal desorption temperature leading to the maximum COP and electric efficiency. Larger salt concentration results in upgraded electrical efficiency and exergy efficiency, and degraded COP. Adsorbents with larger relative pressure where the adsorbent achieves half of the maximum absorption uptake and moderate adsorption enthalpy are more appealing. Solvents with high vaporization latent heat and specific heat capacity contribute to COP, however, decrease electrical efficiency and exergy efficiency. Salts rendering a larger osmotic coefficient improve electric and exergy efficiencies, however degrade the COP. When operating at a desorption temperature of 50 °C, the maximum exergy efficiency can reach 33.9%, meanwhile the electric efficiency and COP are 1.63% and 0.87, respectively.

1. Introduction

Over-exploitation and consumption of fossil energy have induced severe environmental problems. Recognized approaches to meet the shortfall between supply and demand of energy are improving energy efficiency of existing thermodynamic systems and utilizing new and renewable energy resources [1,2]. Meanwhile, with the urbanization of dwellings and the pursuit of thermal comfort in modern economic lifestyles, the demand for cooling is also increasing [3–6]. It is estimated that 72% of primary global energy is discharged into the environment in the form of waste heat [7]. Extracting energy from waste heat paves a promising way to alleviate energy shortages [8–12]. In the world energy background, utilization of low-grade waste heat, a low-cost and widely available alternative energy supply, attracts increasing attention to improve overall energy utilization efficiency [13,14]. However, only a few current “heat-to-power” technologies can be used to harvest the low-grade heat below 80 °C, and the performance is far from satisfactory [15].

Recently, close-looped osmotic heat engines (OHEs) combining membrane distillation (MD) and pressure retarded osmosis (PRO) or reverse electrodialysis (RED) are utilized to recover low-grade heat below 80 °C, which exhibit much higher energy efficiency than most existing traditional “heat to power” technologies [8,16,17]. In the membrane distillation process, driven by the low temperature heat, partial vapor pressure difference at the membrane-liquid interface forces solvent to permeate through the hydrophobic membrane, thus to produce concentrated and diluted salt solutions [18,19]. In the PRO process, originating from the transmembrane osmotic pressure difference, solvent transports from the low concentration side to the pressurized concentrated side, and is then depressurized via a hydro-turbine to generate electricity [20–22]. RED is an electrochemical process that converts the Gibbs free energy of mixing directly into electricity [23–29]. When two streams are fed into the system, the salinity gradient between them drives the ions to transport through the ion

* Corresponding author.
E-mail address: r_long@hust.edu.cn (R. Long).

https://doi.org/10.1016/j.energy.2020.117993
0360-5442/

exchange membranes. And the directed ion movements are converted to electrical current by a redox reaction on the electrode [21,30,31]. Long et al. [32] analyzed the potential application of an OHE that combines with direct contact membrane distillation (DCMD) and RED, and an electrical efficiency of 1.15% was obtained when operating between 20 and 60 °C with 5 M NaCl solution. Tufa et al. [33] experimentally investigated a RED-DCMD system, and a total power density of 0.9–2.4W/m^{2}was obtained. However, DCMD presents extremely high heat transfer loss, which hinders the overall energy efficiency of the DCMD-based OHEs [34]. In order to mitigate heat transfer loss, more advanced MD configurations were developed. Tamburini et al. [14] proposed a reverse electrodialysis heat engine based on RED and multiple effect distillation (MED), and an energy density of 18.3W/m^2 and energy efficiency of 15.4% were achieved. Lee et al. [35] introduced a hybrids system consisting of a multi-stage vacuum membrane distillation (MVMD) and PRO to convert waste heat into electricity with a maximum power density of 9.7 W/m^2.

Adsorption-based heat transformation system are also employed for refrigeration to harvest low-grade heat [36,37]. Jiang et al. [38] employed adsorption-based cooling system incorporated in an Organic Rankine cycle (ORC) for cooling and power cogeneration, which shows the achievability of simultaneous power generation and refrigeration. Zhang and Lior [39] proposed an ammonia-water system combined with absorption cycle to cogenerate refrigeration and power, which consists of an ammonia-water Rankine cycle for generating electricity and an ammonia cycle for providing cooling power. And a thermal and exergy efficiencies of 27.7% and 55.7% were achieved within a maximum operating temperature of 450 °C. Al-Mousawi et al. [40] investigated the impacts of adsorbent materials on power and refrigeration performance. And an energy efficiency of 82% was obtained with AQSOA-Z02 zeolite adsorbent under the heat source temperature of 160 °C. Furthermore, for waste heat below 80 °C, adsorption-based desalination (AD), as a thermal driven desalination method, can be utilized to offer cooling power and produce concentrated solutions that could be used to extract energy in the downstream PRO or RED process. Olkis et al. [41] investigated a hybrid system combining RED and AD for electricity generation from low-grade heat, and an exergy efficiency of 30% was obtained. In their study, the evaporation temperature is set as the same as the condensing temperature, therefore the cooling power is not considered.

In previous studies, although there are many researches on thermally adsorption-based desalination (AD) systems and pressure retarded osmosis (PRO) systems, no literatures have reported the closed-loop system that combines AD and PRO for combined power and cooling cogeneration. In present study, we investigate an adsorption-based cogeneration system that can use low-grade waste heat below 80 °C to provide electricity and offer cooling power. The system is composed of two parts, one is adsorption-based desalination system that generate concentrated solutions as well as produce cooling power by utilizing low-temperature heat energy. The other is the pressure retarded osmosis (PRO) system that converts the Gibbs free energy of mixing of the generated concentrated and diluted salt solutions into electricity. Effects of desorption temperature, salt concentrations, adsorbents, salt types and solvents on the power generation, refrigeration performance and overall efficiency of the system are systematically studied. Criteria for selecting appropriate adsorbents, salts and solvents are analyzed and evaluated. This study could offer an alternative way to convert low-grade heat into electricity and cooling power, and can serve as a guidance for constructing and optimizing such cogeneration systems.

2. Material and methods

2.1. System description

As shown in Fig. 1, the hybrid combined power and cooling cogeneration system consists of an adsorption-based desalination (AD) system for generating concentrated and diluted salt solutions as well as providing cooling power, and a pressure retarded osmosis (PRO) system for converting the Gibbs free energy of mixing of the produced concentrated and diluted salt solutions into electricity. In the adsorption-based desalination system, the solvent is evaporated from the salt solution, absorbing the heat of the refrigerant which provides cooling power to the outside. The evaporated solvent is then absorbed by the adsorbent so that the remaining solution is concentrated. Driven by the external low temperature heat, the solvent is desorbed from the adsorbent and is then condensed in the condenser, generating a diluted solution. In the adsorption-based desalination system, the adsorbent bed needs to go through several states. The adsorbent bed is heated when adsorbate is desorbed, and then is cooled by an external heat sink to ambient temperature for adsorption, enabling a semi-continuous operation, that is, when one bed is adsorbing, the other bed is desorbing. The produced concentrated and diluted solutions enter into the PRO system. Originating from the transmembrane osmotic pressure difference, solvent transports from the low concentration side to the pressurized concentrated side, and is then depressurized to offer electricity through the turbine. To improve the PRO performance, a pressure exchanger is employed to recover the pressure of the effluent permeate solution, as depicted in Fig. 1. The effluents of the PRO system are then mixed, restoring its initial concentration for the next cycle.

2.2. Mathematical modelling and validation

As shown in Fig. 2, the thermodynamic process of the adsorption-based desalination consists of four steps, two for adsorption process (isosteric cooling, isobaric adsorption) and two for desorption process (isosteric heating, isobaric desorption). The working fluid of the adsorption desalination system can be prepared by dissolving salt into pure solvent (water or methanol in present study). The dissolvent salt leads to boiling temperature elevation, and decreased solvent saturated pressure, which can be calculated as $p_{sat,ss} = p_{sat,ps}\exp(-\nu C M_w \Phi)$, where ν is the number of dissociated ions and C is the molarity, M_w is the mole mass, and Φ is the osmotic coefficient. The subscripts ss and ps denote salt solution and pure solution, respectively. The osmotic coefficient Φ can be calculated using the following equation [42].

$$\Phi - 1 = |Z_+ Z_-| f^{\varphi} + m[(2\nu_+\nu_-)/\nu]B^{\varphi} + m^2\left[(2\nu_+\nu_-)^{3/2}\Big/\nu\right]C^{\varphi} \tag{1}$$

where Z is the ion charge, ν is the number of ions. m is the molality. And the other coefficients are listed below [42,43].

$$f^{\varphi} = -A_{\varphi} I^{1/2}\Big/\left(1 + bI^{1/2}\right) \tag{2}$$

$$B^{\varphi} = \beta^{(0)} + \beta^{(1)}\exp\left(-\alpha_1 I^{1/2}\right) + \beta^{(2)}\exp\left(-\alpha_2 I^{1/2}\right) \tag{3}$$

$$A_{\varphi} = (1/3)(2\pi N\rho)^{1/2}\left(e^2\Big/4\pi\varepsilon_0\varepsilon kT\right)^{3/2} \tag{4}$$

where $\beta^{(0)}$, $\beta^{(1)}$, $\beta^{(2)}$, and C^{φ} are Pitzer's ion-interaction parameters. A_{φ} is the Debye-Huckel constant. α_1, α_2, and b are adjustable

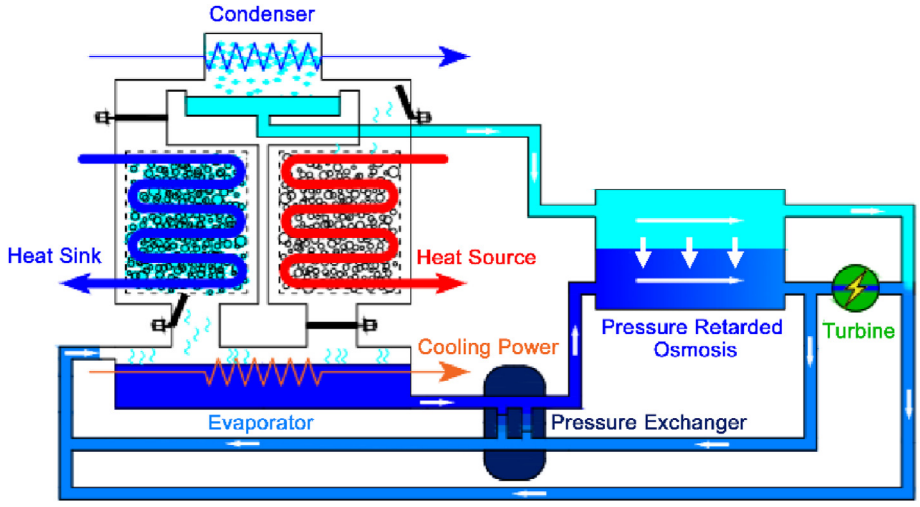

Fig. 1. Schematic diagram of the proposed power and cooling cogeneration system, which consists of an adsorption-based desalination (AD) system for generating concentrated and diluted salt solutions as well as providing cooling power, and a pressure retarded osmosis (PRO) system for converting the Gibbs free energy of mixing of the concentrated and diluted solutions into electricity.

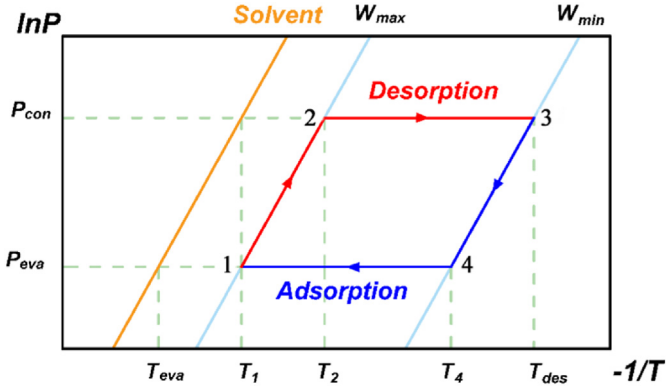

Fig. 2. Schematic diagram of the adsorption cycle. Process 1→3 represents the heating phase (red) and desorption starts from point 2. Process 3→1 represents the cooling phase (blue) and adsorption starts from point 4. (For interpretation of the references to color in this figure legend, the reader is referred to the Web version of this article.)

parameters. I is the ionic strength. N is Avogadro's number. e is the elementary charge, ε_0 is the vacuum permittivity, and k is the Boltzmann constant. ε the relative dielectric constant.

In the AD process, the evaporation temperature is lower than the environment one, thus to absorb heat from the refrigerant and offer cooling power. Therefore, the adsorption pressure is much lower than that of the desorption pressure. The adsorption isotherms are required to characterize the adsorption/desorption processes, which can be described by the Dubinin–Astakhov model [44].

$$W = W_0 \exp\left(-\left(\frac{A}{E}\right)^n\right) \tag{5}$$

where W is the predicted uptake. W_0 is the maximum one. E is the characteristic energy. n is an empirical constant determined by adsorbent particle sizes. A is the Polanyi potential, given by [44].

$$A = RT \ln\left(\frac{p_0(T)}{p}\right) \tag{6}$$

where R is the universal gas constant. P_0 is the saturation pressure at the sorbent temperature T, and p is the adsorption/desorption pressure.

The enthalpy of adsorption can be calculated from adsorption isotherms [45].

$$\Delta_{ads}H_W = R\left(\frac{\partial \ln p}{\partial(1/T)}\right)_W \tag{7}$$

Before the desorption process, the adsorbent should be preheated. Total heat needed Q_{reg} consists of two parts: heat needed in the isosteric heating process $Q_{1-2}$and that in the isobaric desorption processQ_{2-3}. In the isosteric heating process, heat required can be calculated as

$$Q_{1-2} = m_{sb}\int_{T_1}^{T_2} Cp^{eff}(T)dT + m_{sb}\int_{T_1}^{T_2} W_{\max} Cp^{sol}(T)dT \tag{8}$$

and the heat required in the isobaric desorption process can be calculated as

$$Q_{2-3} = m_{sb}\int_{T_2}^{T_3} Cp^{eff}(T)dT + m_{sb}\int_{T_2}^{T_3} \frac{W_{\max}+W_{\min}}{2} Cp^{sol}(T)dT - m_{sb}Q_{soprtion} \tag{9}$$

where $m_{sb}$is the mass of adsorbent, Cp^{eff} is the effective specific heat of the sorbent with heat exchangers considered, which is assumed as the same as specific heat of the sorbent (1 kJ/(kg·K)) in present study. $Cp^{sol}$is the specific heat capacity of adsorbed solvent. W is the uptake of the adsorbent. $Q_{soprtion}$ is the extra energy (sorption heat) needed during the desorption process.

$$Q_{soprtion} = \frac{1}{M_w}\int_{W_{\min}}^{W_{\max}} \Delta_{ads}H(W)dW \tag{10}$$

SEC is a performance parameter that can evaluate the AD system, defined as the energy required per kilogram of solvent $SEC = \frac{Q_{reg}}{m_{sb}\Delta W}$[46], $\Delta W$is the working capacity of the adsorbent. The cogenerated cooling power in the adsorption desalination system can be calculated as $Q_c = m_{sb}H_{ev}\Delta W$, where H_{ev} is the latent heat of vaporization of the solvent.

In the pressure retarded osmosis, driven by the osmotic pressure difference between the diluted and concentrated solutions produced from the AD system, the solvent transports from the low-concentration solution into the pressurized high-concentration one, and is then depressurized via a turbine to generate electricity, as shown in Fig. 1. The concentration of the effluent solution is given by [16,47].

$$C_f = \frac{C_0 V_0}{V_0 + \Delta V} \tag{11}$$

where V_0, C_0 are respectively the inlet volume flow rate and concentration of the draw solution. $\Delta V$is the flow rate of the transmembrane solvent.

When the applied hydraulic pressure equals to the osmotic pressure ($P_{PRO} = \nu R\Phi TC_f$), solvent stops transferring through the membrane. Therefore, the power can be extracted in the PRO process is [16,47].

$$P = P_{PRO}\Delta V = \nu R\Phi T \frac{C_0 V_0}{V_0 + \Delta V}\Delta V \tag{12}$$

According to Eq. (12), the power extracted in the PRO system increases with increasing transmembrane flow rate. As a close-looped system, when the maximum transmembrane flow rate in PRO is equal to the solvent flow rate generated in the adsorption-based desalination system ($\Delta V = \Delta W m_{sb}$), the power extracted in the PRO system achieves its maximum value. And the outlet solution concentration of the PRO system is equal to the initial concentration in the adsorption-based desalination system ($C_f = C_1$). At this point, the corresponding applied pressure in the PRO system is $P_{PRO} = \nu R\Phi TC_1$. The maximum work extractable is $W_{PRO} = \nu R\Phi T_1 C_1 \Delta W m_{sb}$.

Overall, the proposed hybrid cogeneration system for low temperature heat harvesting can offer electricity and cooling power simultaneously. For electricity supply, the electric efficiency is employed to evaluate the power generation performance, which is calculated as

$$\eta_e = \frac{W_{PRO}}{Q_{reg}} = \frac{\nu R\Phi T_1 C_1 \Delta W}{Q_{1-2} + Q_{2-3}} \tag{13}$$

As a refrigerator, the coefficient of performance (COP) is adopted to measure the refrigeration performance of the hybrid system, which is defined as

$$COP = \frac{Q_c}{Q_{reg}} = \frac{m_{sb}H_{ev}\Delta W}{Q_{1-2} + Q_{2-3}} \tag{14}$$

The total energy recovery rate can be defined as

$$\eta_Q = \frac{W_{PRO} + Q_c}{Q_{reg}} = \frac{\nu R\Phi T_1 C_1 \Delta W + m_{sb}H_{ev}\Delta W}{Q_{1-2} + Q_{2-3}} \tag{15}$$

Eq. (15) assumes energy quality of the electricity and cooling power are the same. However, the energy quality of the electricity is much larger than that of the cooling power. Therefore, the total energy recovery rate could not present the real energy utilization degree. Here we employ the exergy efficiency to evaluate the performance of the hybrid cogeneration system. The total useful energy is the sum of the produced electricity and the cryogenic exergy that is calculated as $Q_c(T_{eva}/T_{ev} - 1)$, where T_{ev} and T_{eva} are the environmental temperature and evaporation temperature respectively. The exergy efficiency of the hybrid co-generation system is

$$\eta_{ex} = \frac{Q_c\left(\frac{T_{eva}}{T_{ev}} - 1\right) + W_{PRO}}{Q_{reg}\left(1 - \frac{T_{ev}}{T_{des}}\right)} \tag{16}$$

where T_{des} is the desorption temperature.

The validation of the present model on the cooling performance is conducted. Fig. 3 shows the comparison of the COP in present calculation and that of Lange et al. [48]. Here pure methanol is employed as the working fluid and ZIF-8 as the adsorbent. The evaporation temperature and condensation temperature are 278 K and 303 K, respectively. The adsorption temperature is the same with the condensation one. The prediction from the present model is in very good agreement with the COP based on measured adsorption isotherms [48], which validates the model in present study.

2.3. Adsorbents selection

Activated carbons (ACs) and Metal-organic frameworks (MOFs) are widely used for methanol and water adsorption. 20 kinds of AC and MOF adsorbents commercially available and extensively investigated in previous studies are selected in present study. The adsorption uptakes for the selected adsorbents are listed in Table A1 in the Appendix.

2.4. Salt solution selection

Different salt solutions have different the osmotic coefficients, which impacts the evaporation pressure in the evaporator that determines the desalination characteristics and the cooling power, and the osmotic pressure difference in the pressure retarded osmosis that impacts the power extracted. Here, five extensively investigated salts in previous studies are chosen to prepare the

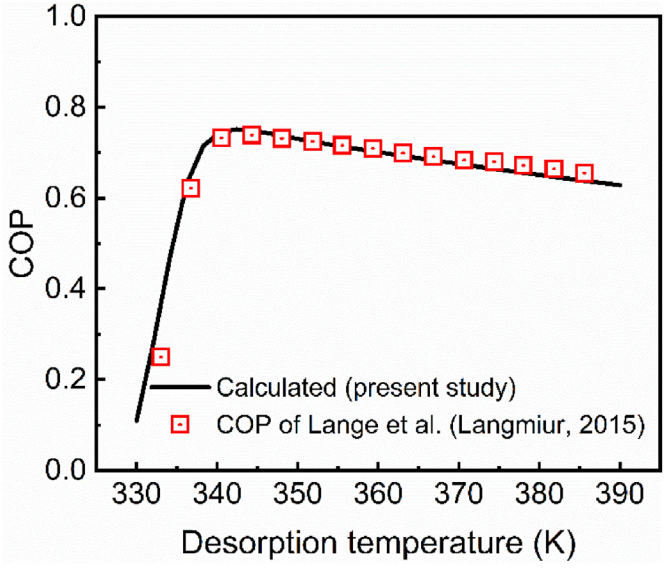

Fig. 3. Comparison of the COP in present calculation and that of Lange et al. [48].

working salt solution, *i.e.* NaI, LiBr, LiCl, NaSCN and $LiNO_3$. In addition, the impacts of different solvents such as water and methanol are also discussed. To calculate the osmotic coefficient Φ, Pitzer parameters for methanol and water solutions used in present study are listed in Table 1.

2.5. Physical properties of solvents

The densities of MeOH and water and relative dielectric constants can be calculated as [52–55].

$$\rho_{MeOH} = \exp\left(A + BT + CT^2\right) \tag{17}$$

$$\rho_{water} = A + BT + CT^2 + DT^3 \tag{18}$$

$$\varepsilon = a + bT + cT^2 + dT^3 \tag{19}$$

And the relevant parameters in Eq. (17)- (19) are listed in Table 2 and Table 3.

2.6. Operation conditions

The adsorption isotherms of the adsorbents are significantly impacted by the desorption and adsorption temperatures, and the evaporation and condensing temperatures. To function as a refrigerator, the performance of the hybrid cogeneration system is also impacted by the evaporation temperature in the AD process. In the calculation, the evaporation temperature is fixed at 288.15 K, the condensing temperature is the same as the environmental temperature (293.15 K). The desorption temperature varies from 313.15 K to 363.15 K to evaluate of the impacts of desorption temperature on the performance of the hybrid system.

3. Results and discussion

3.1. The effect of operation conditions

We first investegate the effect of desorption temperature on the hybrid adsorption-based cogeneration system. Here LiBr-methanol is employed as the working fluid and AC-LSZ30 as the absorbent. The evaporation and condensation temperatures are maintained at 288.15 K and 293.15 K, respectively. As shown in Fig. 4a, the adsorption working capacity increases with increasing desorption temperatures for the decrease of the minimum absorption uptake at higher temperatures (Fig. 4e). Therefore, the cooling power and work extracted increase with increasing desorption temperatures (Fig. 4b–c). Both increased adsorption working capacity and elevated temperature are responsible for much obvious augmentation of the regeneration heat (Fig. 4d). It can also be seen from Fig. 4a that the working capacity of the adsorbent decreases with the increasing concentration of the working solution. Higher working concentration lowers the evaporation pressure and further reduces the maximum adsorption uptake, thus the adsorption working capacity (Fig. 4f), resulting in decreased cooling power. Although the working capacity of the adsorbent decreases with increasing concentration, the work of extraction is increased (Fig. 4c). The increase of the working concentration augments the transmembrane osmotic pressure difference, which overrides the impacts of the decreases working capacity, leading to increased work extracted.

Fig. 5 shows the COP, electric efficiency, energy recovery rate, and exergy efficiency of the hybrid adsorption-based cogeneration system. As shown in Fig. 5a and b, the COP and η_e first increase with increasing desorption temperature, reaches their maximum values, and then decreases. At lower desorption temperatures, the cooling power and electric power increases with increasing desorption temperatures. As the increasement of the working capacity is much larger than that of the regeneration heat, the electric efficiency and the COP increase with increasing desorption temperatures, as shown in Fig. 4a and d. At higher desorption temperatures, the regeneration heat acts dominantly, therefore, the electric efficiency and the COP decreases with increasing desorption temperatures. According to Eq. (15), the energy recovery rate exhibits the same behavior with the COP or electric efficiency as the desorption temperature increases. Larger working concentration increases the electric efficiency. However, it decreases the COP and energy recovery rate for increased work extracted and reduced cooling power at larger salt concentrations (Fig. 4b–c). As the cooling power is much larger than the work extracted, larger working concentration significantly reduces the cooling power, thereby the energy recovery rate, as depicted in Fig. 5c.

To step further, the quality of cold energy is lower than that of work, while the heat recovery rate only considers the quantity of energy and ignores the quality. A more reasonable useful energy of the hybrid cogeneration system should be the electricity and cryogenic exergy. Exergy efficiency should be more appropriate to evaluate the overall performance of the hybrid cogeneration system, which is defined as the total exergy output divided by the input heat exergy (Eq. (16)). As shown in Fig. 5d, the exergy efficiency decreases with increasing desorption temperatures due to much obviously augmented heat exergy consumption at higher desorption temperatures. Although the cooling power decreases with increasing working concentrations, its cryogenic exergy increases. The exergy efficiency of the hybrid cogeneration system increases with increasing working concentrations.

Table 1
Pitzer parameters for solutions studied in this work.

Salt	Solvent	$\beta^{(0)}$	$\beta^{(1)}$	$\beta^{(2)}$	C^{φ}	Ref
LiCl	Methanol	−0.11458	−3.95303	3.421	0.06478	[49]
LiBr	Methanol	0.00275	−2.6665	2.238	0.05542	[49]
NaSCN	Methanol	0.19224	1.39440	−1.202	−0.01017	[50]
NaI	Methanol	0.40830	1.04430	−0.875	−0.02224	[50]
$LiNO_3$	Methanol	0.003768	0.465495	−26.295126	0.045220	[51]
LiCl	Water	0.1494	0.3047		0.00359	[42]
LiBr	Water	0.1748	0.2547		0.0053	[42]
NaSCN	Water	0.1005	0.3582		−0.00303	[42]
NaI	Water	0.1195	0.3439		0.0018	[42]
$LiNO_3$	Water	0.1420	0.2780		−0.00551	[42]

3.2. The effect of adsorbents

As the salt solution separation and cooling power supply lie in the adsorption-based desalination process, the chemical and physical characteristics of the adsorbent present a determined role on the performance of the proposed hybrid cogeneration system. Here twenty kinds of adsorbent are considered in present study. The desorption and adsorption temperaures are set at 333.15 K and 288.15 K, respectivily. LiBr-Methanol solution at 3 mol/kg is employed as the working fluid. Fig. 6 presents the COP, electric efficiency, exergy efficiency, and the relevant detailed parameters under various adsorbents. The adsorbent AC MAXSSORB3 leads to largest COP, electric efficiency, and exergy efficiency simultaneously for the largest extracted work and cooling power due to largest adsorption working capacity (Fig. 6d–f). Their minimum values are obtained under the adsorbent ACF KF-1000 for least

Table 2
Coefficients A, B, C and D to calculate the density [54,55].

solvent	A	B/K^{-1}	C/K^{-2}	D/K^{-3}
water	658.6	3.4537	-0.99533×10^{-2}	0.73989×10^{-5}
MeOH	0.08584	-9.60×10^{-4}	-4.30×10^{-7}	

Table 3
Coefficients a, b, c and d to calculate relative dielectric constant [52,53].

solvent	a	10^2b	10^4c	10^7d
water	87.727	−39.81	8.699	−7.948
MeOH	37.909	−22.838	6.659	

working capacity. There is a strict negative correlation between the SEC and the exergy efficiency. The larger the SEC, the less energy consumption to guarantee a desired adsorption working capacity, and thus the smaller the efficiency.

Key parameters of the adsorbents impacting the adsorption process are relative pressure α, where the adsorbent achieves half of the maximum absorption uptake and the adsorption enthalpy. Fig. 7 presents the relationship of the exergy efficiency, adsorption working capacity, α and the adsorption enthalpy. The exergy efficiency increases with the increase of adsorption working capacity and remains unchanged when ΔW is larger than a certain value (0.3 g/g in present study). There exists a positive correlation between α and exergy efficiency, and lager α leads to higher exergy efficiency. However, neither higher nor lower adsorption enthalpy can guarantee the maximum exergy efficiency. A moderate adsorption enthalpy between 1.2 MJ/kg and 1.3 MJ/kg results in a higher exergy efficiency up to 24%. Therefore, a qualified adsorbent should have higher α and moderate adsorption enthalpy (1.2 MJ/kg~1.3 MJ/kg).

3.3. The effect of salts

Different salt solutions have different the osmotic coefficients, which impacts the evaporation pressure in the evaporator that determines the desalination characteristics and the cooling power, and the osmotic pressure difference in the pressure retarded osmosis that impacts the power extracted. Here solutions with various salts (NaI, LiBr, LiCl, NaSCN and $LiNO_3$) dissolving in the methanol are used to prepare the working fluid of the hybrid cogeneration system. The concentration of the working solution is set at 3 mol/kg. The desorption and adsorption temperaures are fixed at 333.15 K and 288.15 K, respectivily. As shown in Fig. 8, larger osmotic coefficient leads to smaller evaporation pressure, resulting in decreased maximum absorbing uptake in the adsorption process and the adsorption working capacity (Fig. 8a). The osmotic coefficient of the NaI−MeOH solution is the largest, leading to the least evaporation pressure and adsorption working capacity. Therefore, the regeneration heat and cooling power with the NaI−MeOH solution present smallest values. However, the extracted work exhibits the largest value based on the fact that the impact of the osmotic coefficient on the power output overrides the impact of the decreased adsorption working capacity. Hence the electric

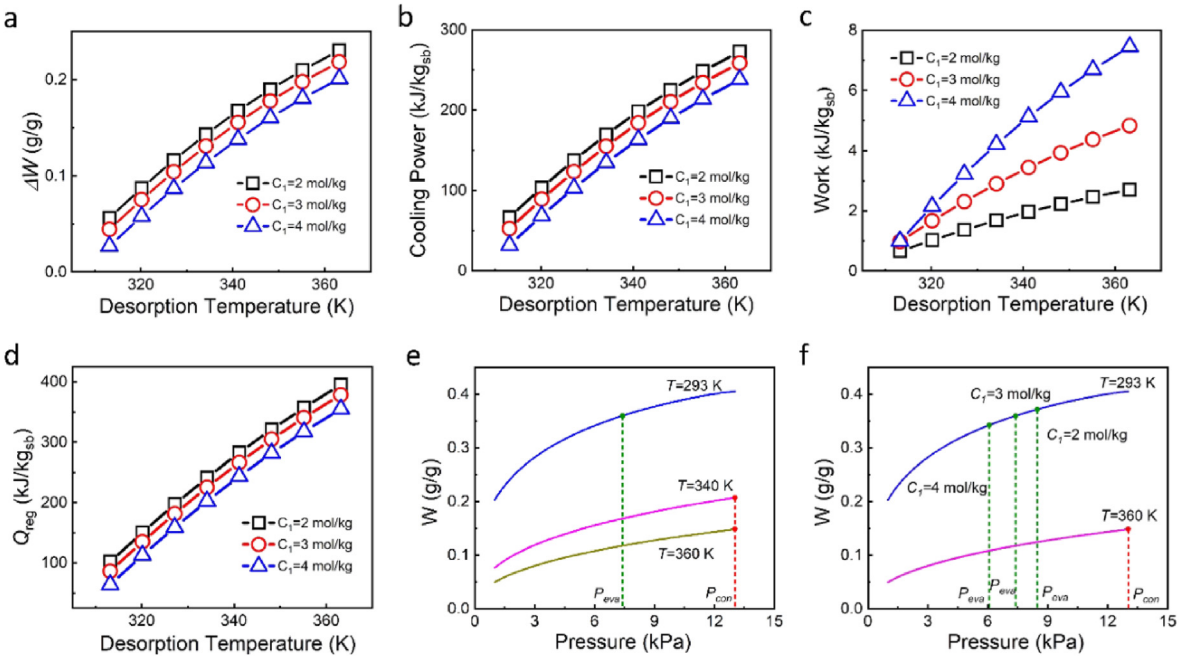

Fig. 4. Work capacity of the absorption-based desalination system (a), cooling power (b), work extracted (c), heat absorbed (d) and adsorption uptake (e, f) under different desorption temperatures and working concentrations.

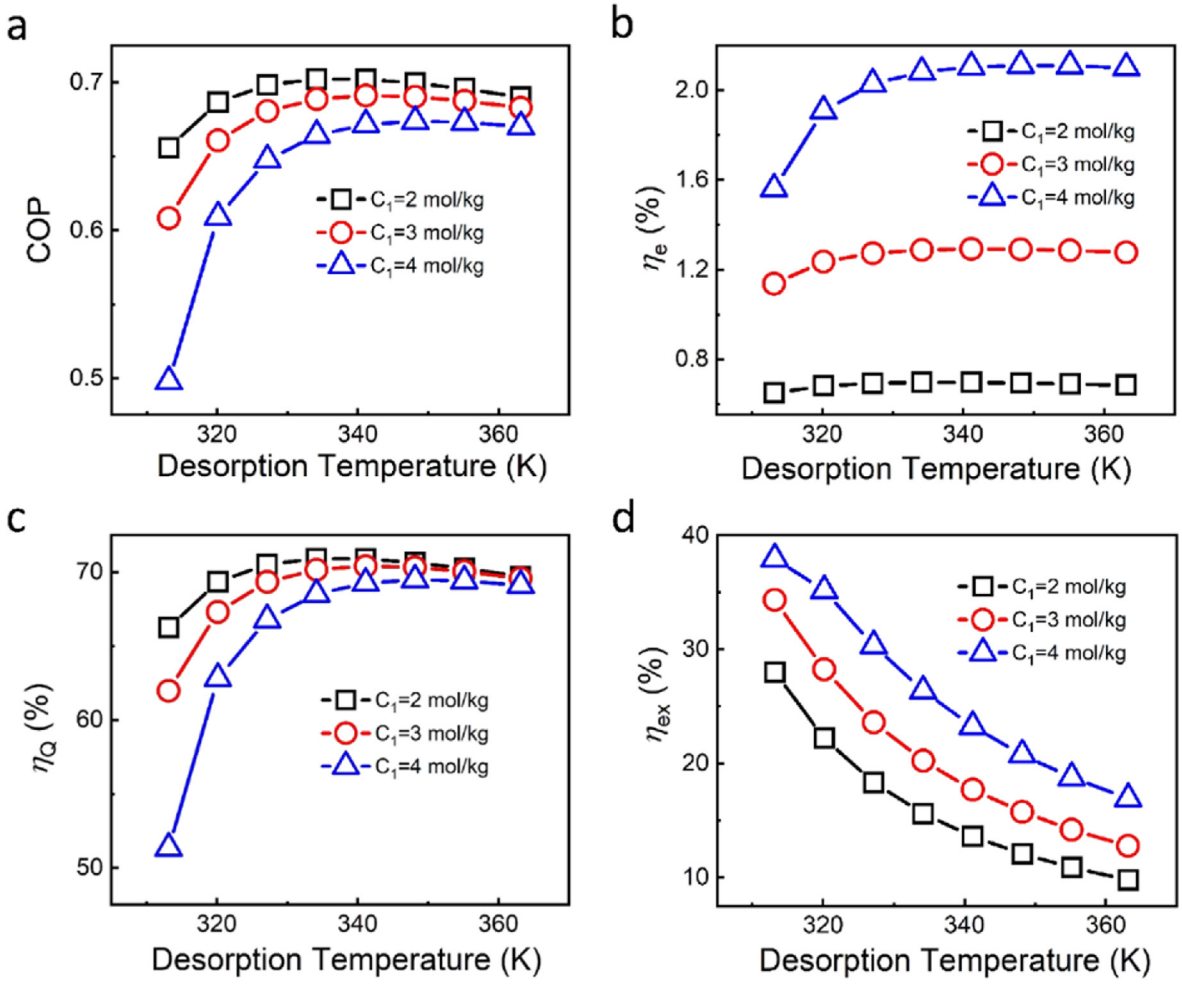

Fig. 5. Coefficient of performance (a), electric efficiency (b), energy recovery rate (c), and exergy efficiency (d) under different desorption temperatures and working concentrations.

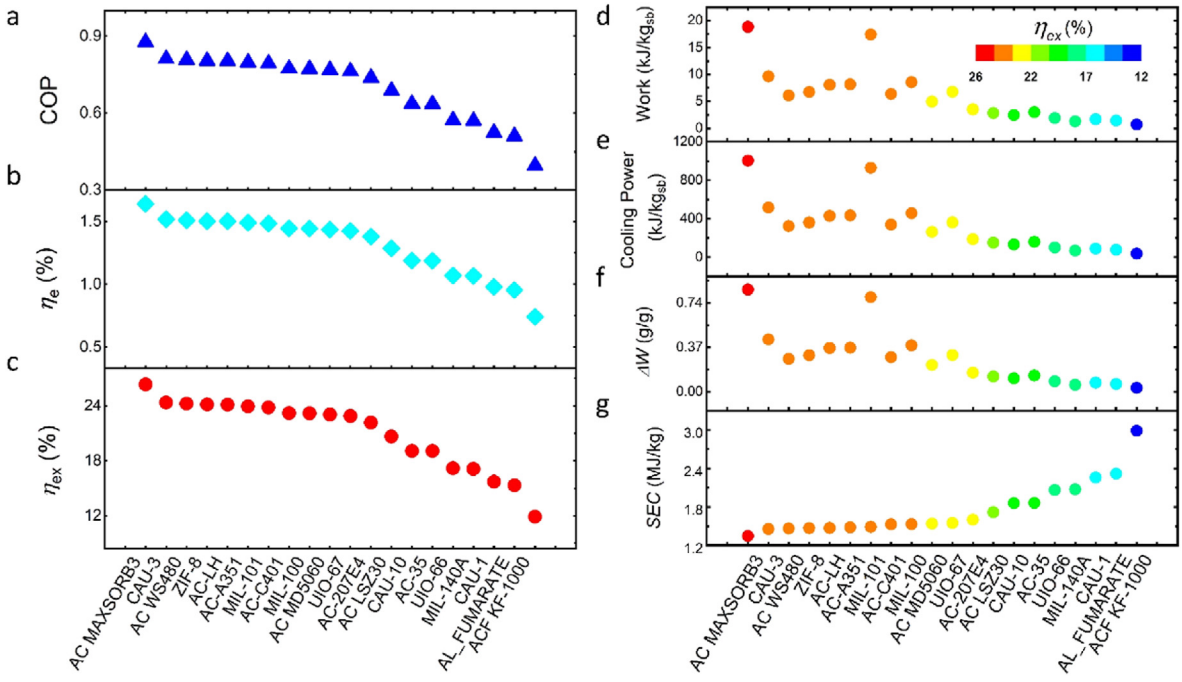

Fig. 6. COP (a), electric efficiency (b), exergy efficiency (c), work extracted (d), cooling power (e), working capacity (f) and SEC (g) under various absorbents. (d–g) are colored by exergy efficiency.

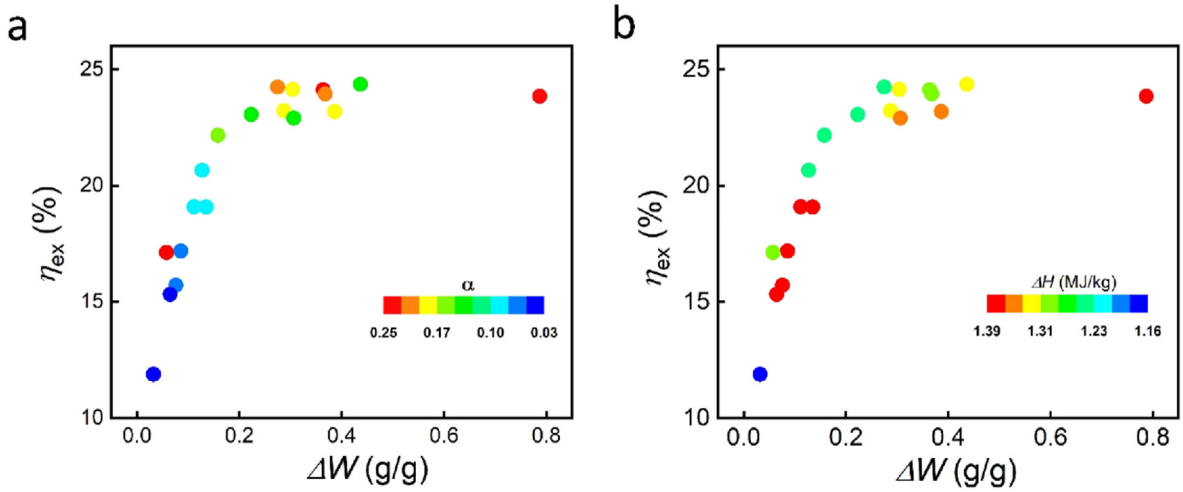

Fig. 7. The relation of the exergy efficiency with the working capacity for different adsorbents. (a) colored by α, and (b) is colored by adsorption enthalpy.

efficiency with NaI−MeOH solution employed as the working fluid is the largest, and that with $LiNO_3$−MeOH solution is the least, as shown in Fig. 9. However, the COP presents an opposite trend. The COP with $LiNO_3$−MeOH solution is the largest for significantly decreased regeneration heat. Due to significant exergy consumption, solutions with larger osmotic coefficients lead to higher exergy efficiency, as depicted in Fig. 9b. The exergy efficiency with NaI−MeOH solution employed as the working fluid is the largest. Overall, salt solutions with larger osmotic coefficient are preferred to achieve a desirable overall performance of the proposed hybrid co-generation system.

3.4. The effect of solvents

We furhter investigate the impacts of the solvents on the performance of the hrbrid co-generation system. Here we emloy LiBr-water solution and LiBr-Methanol solution as the working fluids. The working concentration varies from 2 to 5 mol/kg, and CAU-10 is

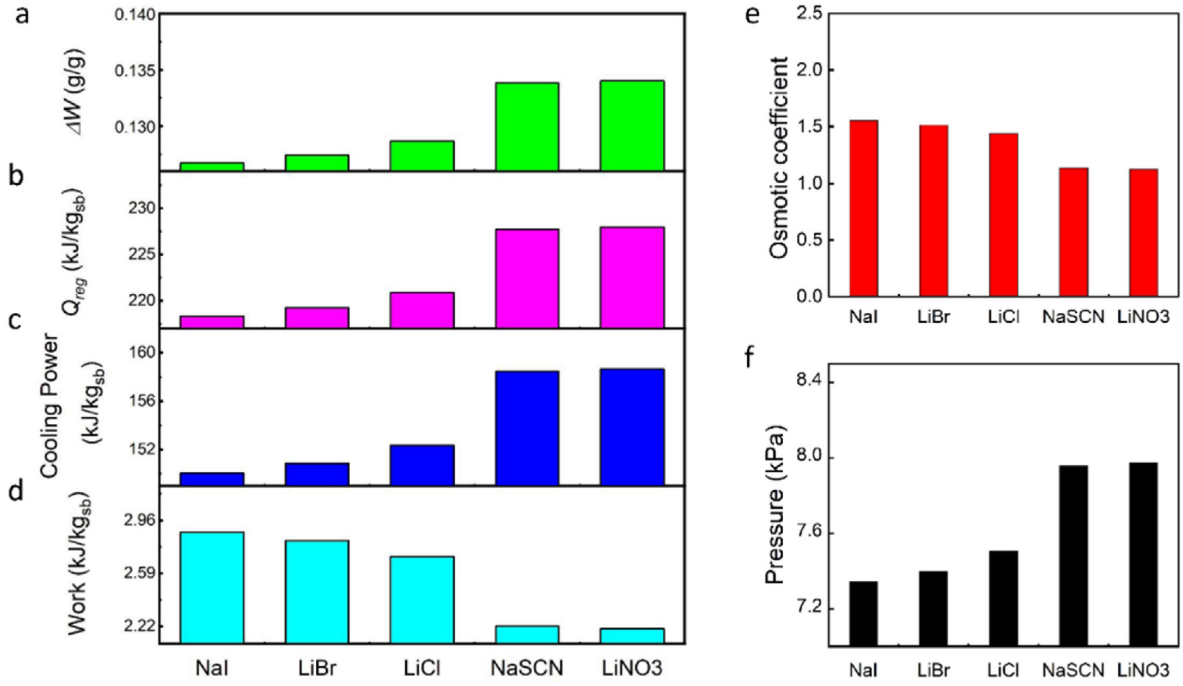

Fig. 8. Working capacity (a), heat adsorbed (b), cooling power (c), work extracted (d) under various salts. (e, f) Osmotic coefficient and evaporation pressure under different salts.

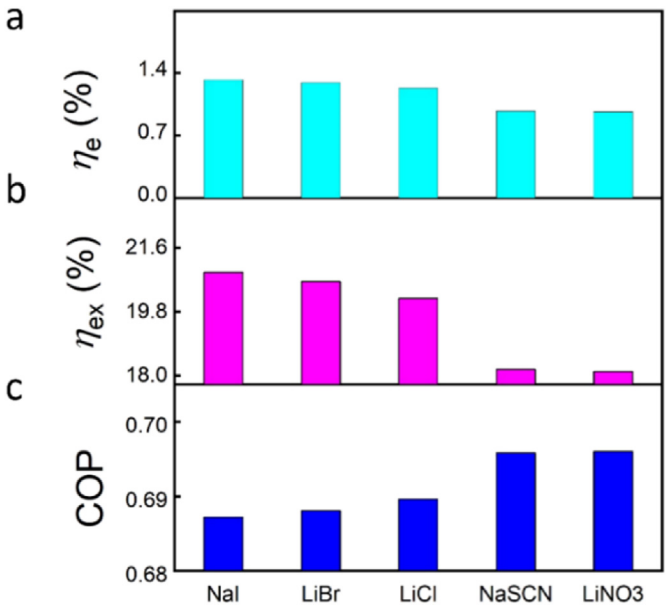

Fig. 9. Electric efficiency (a), exergy efficiency (b) and COP (c) under different salts.

chosen as the adsorbent. The desorption and adsorption temperaures are fixed at 333.15 K and 288.15 K, respectivily. As the adsorpiton uptake for water is much larger than that for methanol for the selected adsorbent, the adsorption working capacity with methanol as the solvent is less than that with water as the solvent, as shown in Fig. 10. Therefore the work and cooling power present larger values with water employed as the solvent. Larger heat capacity and adsorption working capacity induces a much augment of the rengeration heat. As shown in Fig. 11, the SEC with water as the solvent is much larger than that with methanol as the solvent, leading to a lower electric efficiency. As the augment of the cooling power induced by enhanced adsorption working capacity is much less than that of the regeneration heat, leading to a lower COP when water is chosen as the solvent. Based on the fact that LiBr-water working fluid corresponds to larger cryogenic exergy and electricity, at lower working concentrations, the exergy efficiency with LiBr-water as the working fluid exhibits a larger value than that with LiBr−MeOH as working fluid. At high concentrations, exergy consumption with LiBr-water as the working fluid is much larger than that with LiBr-methanol as the working fluid. The exergy efficiency with LiBr-methanol as the working fluid exhibits a much larger value. Therefore, a satisfied solvent is concentration depended.

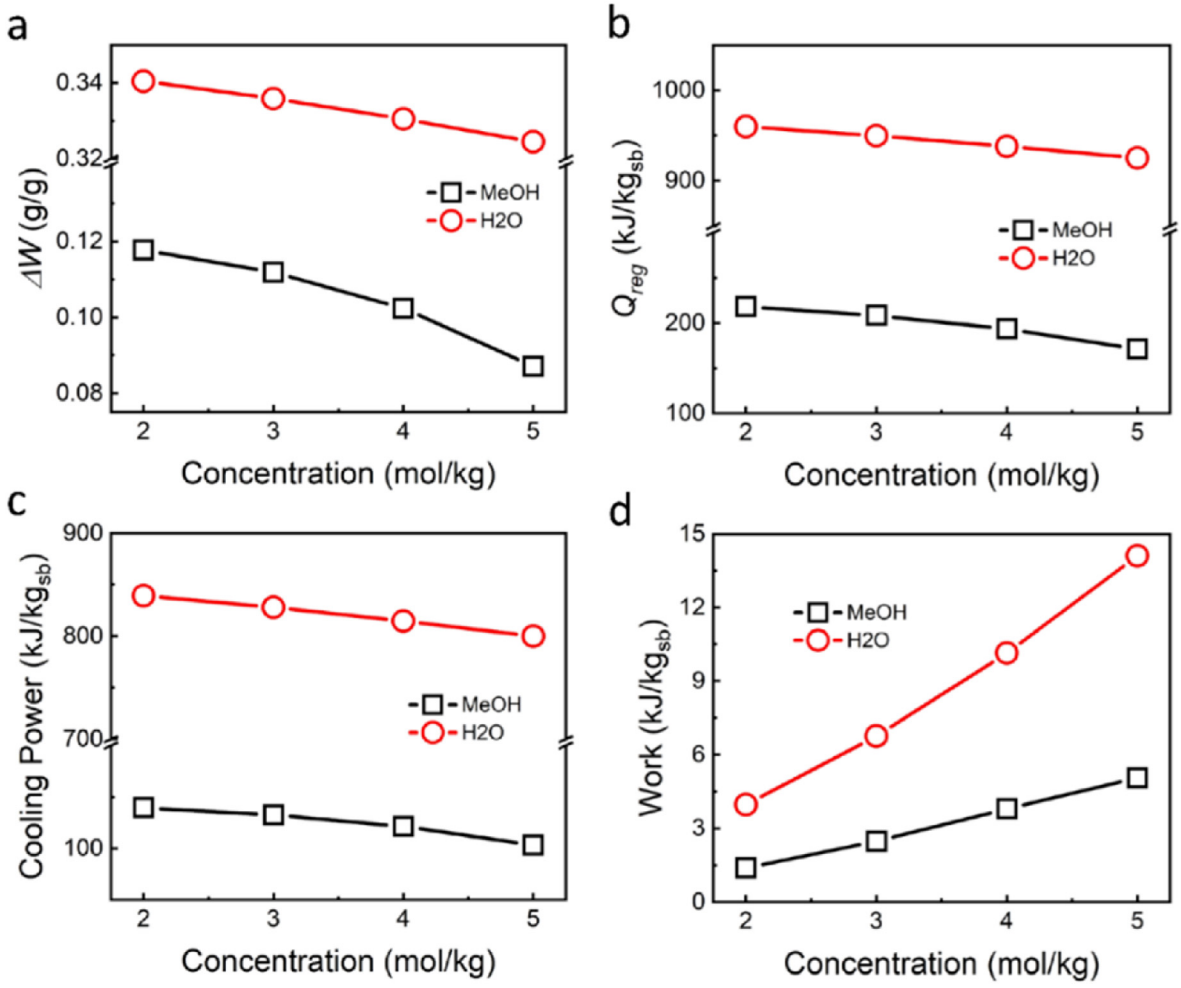

Fig. 10. Working capacity (a), heat adsorbed (b), cooling power (c), and work extracted (d) under various working concentrations.

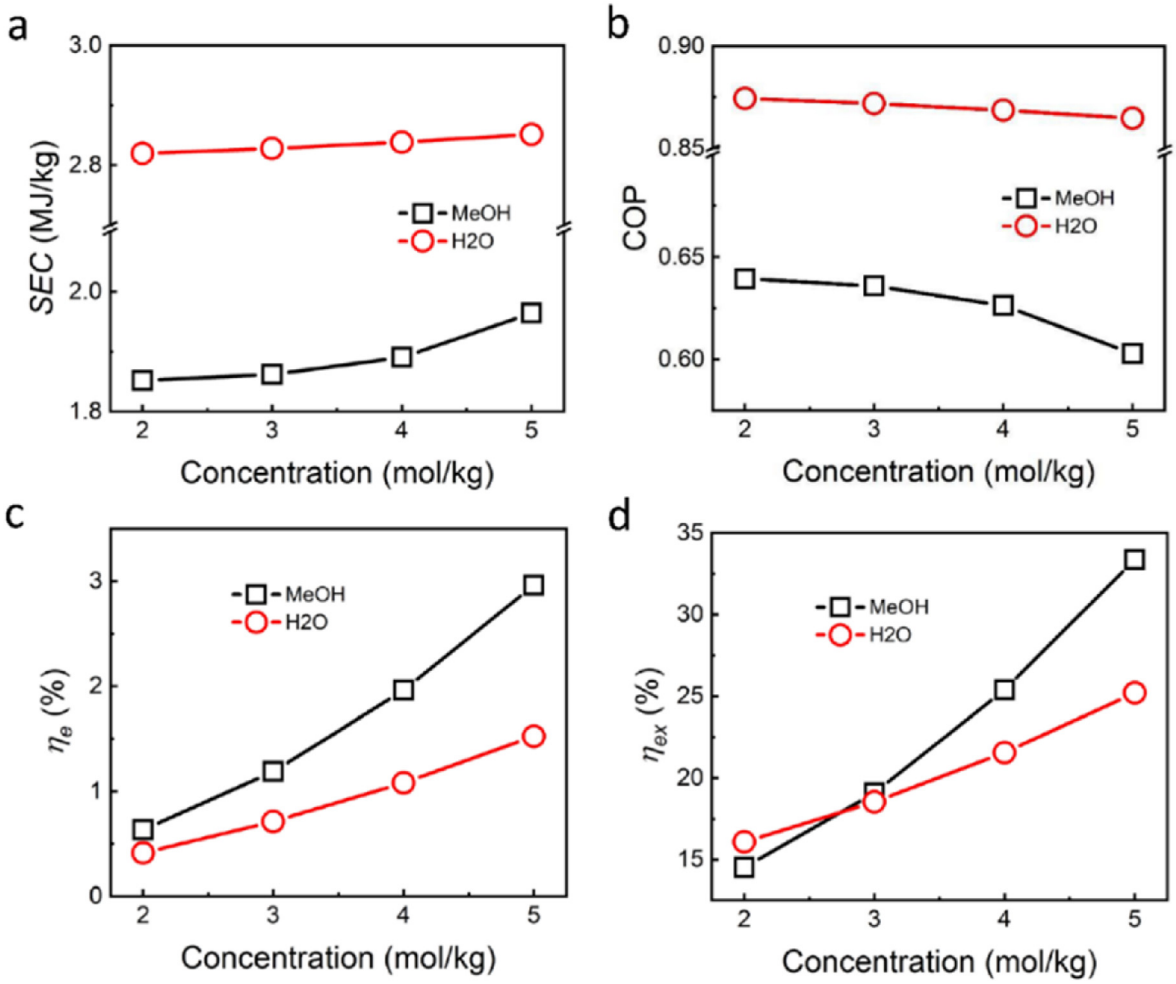

Fig. 11. SEC (a) of the adsorption-based desalination system, COP (b), electric efficiency (c), and exergy efficiency (d) under various working concentrations.

4. Conclusions

In this study, a novel adsorption-based power and cooling cogeneration system is investigated for low-grade heat (<80 °C) energy harvesting, which consists of an adsorption-based desalination system that provides cooling power and produce concentrated and diluted solutions, and a PRO system that generates electricity from the produced high and low concentration solutions. Exergy efficiency is introduced to evaluate the overall system performance, considering the difference of electricity and cooling power in energy quality. Effects of desorption temperature, salt concentrations, adsorbents, salt types and solvents on the performance of the proposed adsorption-based cogeneration system are investigated. Results reveal that the SEC and exergy efficiency show a strict negative correlation. Larger salt concentration results in upgraded electrical efficiency and exergy efficiency, and degraded COP. Adsorbents with larger relative pressure where the adsorbent achieves half of the maximum absorption uptake and proper adsorption enthalpy are more appealing. Solvents with high vaporization latent heat and specific heat capacity contribute to COP, however, decrease electrical efficiency and exergy efficiency. Salts rendering a larger osmotic coefficient improve the electric and exergy efficiencies, however degrade the COP. When operating at a desorption temperature of 50 °C, the maximum exergy efficiency can reach 33.9% with 3 M LiBr-methanol as the working solution and AC MAXSORB3 as the adsorbent, meanwhile the electric efficiency and COP are 1.63% and 0.87, respectively.

Unlike traditional close-looped osmotic heat engines such as RED-DCMD and PRO-DCMD only for electricity generation, present hybrid power and cooling cogeneration system exhibits a much higher overall performance, offering a new way to efficiently harvest low temperature waste heat. Furthermore, theoretically, the heat that cools the adsorbent bed and the latent heat released by the solvent in the condenser could be used to compensate part of the heat needed to heat the adsorbent, which could significantly augment the system performance. Further efforts on developing new configurations that involve heat recovery are appealing.

Declaration of competing interest

The authors claim that there are no conflicts to declare.

CRediT authorship contribution statement

Yanan Zhao: Writing - original draft, Visualization. **Zuoqing Luo:** Formal analysis. **Rui Long:** Methodology, Writing - review & editing, Funding acquisition. **Zhichun Liu:** Formal analysis. **Wei Liu:** Conceptualization, Funding acquisition.

Acknowledgements

This work was financially supported by the National Natural

Science Foundation of China (51706076, 51736004).

Appendix A. Supplementary data

Supplementary data to this article can be found online at https://doi.org/10.1016/j.energy.2020.117993.

Appendix

Table A1
Adsorption uptakes for Methanol and water studied in this work

Adsorbent + Solvent	Uptake equation	Ref
AC LSZ30+MeOH	$w = 0.405 \exp\left(-3.1972 \times 10^{-4}\left(T \ln\left(\frac{p_s}{p}\right)\right)^{1.16}\right)$	[56]
AC MAXSORB3+MeOH	$w = 1.24 \exp\left(-4.022 \times 10^{-6}\left(T \ln\left(\frac{p_s}{p}\right)\right)^{2}\right)$	[57]
AC MD5060+MeOH	$w = 0.535 \exp\left(-4.5895 \times 10^{-5}\left(T \ln\left(\frac{p_s}{p}\right)\right)^{1.5}\right)$	[56]
AC WS480+MeOH	$w = 0.49 \exp\left(-2.8 \times 10^{-5}\left(T \ln\left(\frac{p_s}{p}\right)\right)^{1.65}\right)$	[58]
AC-207E4+MeOH	$w = 0.365 \exp\left(-1.4962 \times 10^{-4}\left(T \ln\left(\frac{p_s}{p}\right)\right)^{1.34}\right)$	[56]
AC-35+MeOH	$w = 0.425 \times 10^{-3}\rho_r \exp\left(-5.02 \times 10^{-7}\left(T \ln\left(\frac{p_s}{p}\right)\right)^{2.15}\right)$	[59]
AC-A351+MeOH	$w = 0.786 \times 10^{-3}\rho_r \exp\left(-\left(\frac{RT}{4810}\ln\left(\frac{p_s}{p}\right)\right)^{1.76}\right)$	[60]
AC-C401+MeOH	$w = 0.633 \times 10^{-3}\rho_r \exp\left(-\left(\frac{RT}{5118}\ln\left(\frac{p_s}{p}\right)\right)^{1.85}\right)$	[60]
ACF KF-1000+MeOH	$w = 0.307\frac{36.98\frac{p}{p_s}}{1+36.98\frac{p}{p_s}}$	[61]
AC-LH + MeOH	$w = 0.860 \times 10^{-3}\rho_r \exp\left(-2.574 \times 10^{-4}\left(T \ln\left(\frac{p_s}{p}\right)\right)^{1.321}\right)$	[59]
AL-FUMARATE + MeOH	$w = \frac{\rho_r}{1000}\left[\frac{0.3381}{1+\exp(0.0006354(F-8270))} + 0.09542\exp(-0.0009661F - 1.046\times10^{-6}F + 0.03327)\right]$	[62]
CAU-1+MeOH	$w = \frac{\rho_r}{1000}\left[\frac{0.3758}{1+\exp(0.001419(F-7052))} + 0.1012\exp(-0.0006468F - 3.378\times10^{-6}F + 0.08771)\right]$	[62]
CAU-10+MeOH	$w = \frac{\rho_r}{1000}\left[\frac{0.4148}{1+\exp(0.0004027(F-5344))}\right]$	[62]
CAU-3+MeOH	$w = \frac{\rho_r}{1000}\left[\frac{0.4319}{1+\exp(0.007538(F-4779))} + 0.3095\exp(-0.0002375F)\right]$	[62]
MIL-100+MeOH	$w = \frac{\rho_r}{1000}\left[\frac{0.1338}{1+\exp(0.003354(F-5342))} + \frac{0.1015}{1+\exp(0.0005431(F-13,800))} + 0.1105\exp(-0.0004114F)\right]$	[62]
MIL-101+MeOH	$w = \frac{\rho_r}{1000}\left[\frac{0.3764}{1+\exp(0.00167(F-3545))} + 0.4565\exp(-0.0001052F)\right]$	[62]
MIL-140A + MeOH	$w = \frac{\rho_r}{1000}\left[\frac{0.742}{1+\exp(0.002408(F-3089))} + 0.8161\exp(-0.0001144F)\right]$	[62]
UIO-66+MeOH	$w = \frac{\rho_r}{1000}\left[\frac{0.1401}{1+\exp(0.00246(F-6803))} + 0.122\exp(-0.00017F)\right]$	[62]
UIO-67+MeOH	$w = \frac{\rho_r}{1000}\left[\frac{0.1648}{1+\exp(0.001395(F-6602))} + 0.2602\exp(-0.0001055F)\right]$	[62]
ZIF-8+MeOH	$w = \frac{\rho_r}{1000}\left[\frac{0.4295}{1+\exp(0.0157(F-4895))} + 0.2852\exp(-0.0001874F)\right]$	[62]
CAU-10+water	$w = \left[\frac{0.27}{1+\exp(0.02276(F-4535))} + 0.0088\exp(-0.0003765F)\right]\frac{\rho_r}{1000}$	[63]

References

[1] Chu S, Majumdar A. Opportunities and challenges for a sustainable energy future. Nature 2012;488(7411):294–303.
[2] Barkhordarian O, Behbahaninia A, Bahrampoury R. A novel ammonia-water combined power and refrigeration cycle with two different cooling temperature levels. Energy 2017;120:816–26.
[3] Tamm G, Goswami DY, Lu S, Hasan AA. Novel combined power and cooling thermodynamic cycle for low temperature heat sources, Part I: theoretical investigation. Journal of Solar Energy Engineering, Transactions of the ASME 2003;125(2):218–22.
[4] Thu K, Saha BB, Chua KJ, Ng KC. Performance investigation of a waste heat-driven 3-bed 2-evaporator adsorption cycle for cooling and desalination. Int J Heat Mass Tran 2016;101:1111–22.
[5] Padilla RV, Demirkaya G, Goswami DY, Stefanakos E, Rahman MM. Analysis of power and cooling cogeneration using ammonia-water mixture. Energy 2010;35(12):4649–57.
[6] Zare V, Mahmoudi SMS, Yari M, Amidpour M. Thermoeconomic analysis and optimization of an ammonia–water power/cooling cogeneration cycle. Energy 2012;47(1):271–83.
[7] Forman C, Muritala IK, Pardemann R, Meyer B. Estimating the global waste heat potential. Renew Sustain Energy Rev 2016;57:1568–79.
[8] Kwon K, Park BH, Kim DH, Kim D. Parametric study of reverse electrodialysis using ammonium bicarbonate solution for low-grade waste heat recovery.

Energy Convers Manag 2015;103:104–10.
[9] Luo X, Cao X, Mo Y, Xiao K, Zhang X, Liang P, et al. Power generation by coupling reverse electrodialysis and ammonium bicarbonate: implication for recovery of waste heat. Electrochem Commun 2012;19:25–8.
[10] Hung TC, Shai TY, Wang SK. A review of organic rankine cycles (ORCs) for the recovery of low-grade waste heat. Energy 1997;22(7):661–7.
[11] Shaulsky E, Boo C, Lin S, Elimelech M. Membrane-based osmotic heat engine with organic solvent for enhanced power generation from low-grade heat. Environ Sci Technol 2015;49(9):5820–7.
[12] Bao H, Wang Y, Charalambous C, Lu Z, Wang L, Wang R, et al. Chemisorption cooling and electric power cogeneration system driven by low grade heat. Energy 2014;72:590–8.
[13] Peris B, Navarro-Esbrí J, Molés F. Bottoming organic Rankine cycle configurations to increase Internal Combustion Engines power output from cooling water waste heat recovery. Appl Therm Eng 2013;61(2):364–71.
[14] Tamburini A, Tedesco M, Cipollina A, Micale G, Ciofalo M, Papapetrou M, et al. Reverse electrodialysis heat engine for sustainable power production. Appl Energy 2017;206:1334–53.
[15] Nuwayhid RY, Shihadeh A, Ghaddar N. Development and testing of a domestic woodstove thermoelectric generator with natural convection cooling. Energy Convers Manag 2005;46(9):1631–43.
[16] Lin S, Yip NY, Cath TY, Osuji CO, Elimelech M. Hybrid pressure retarded osmosis–membrane distillation system for power generation from low-grade heat: thermodynamic analysis and energy efficiency. Environ Sci Technol 2014;48(9):5306–13.
[17] Giacalone F, Vassallo F, Griffin L, Ferrari MC, Micale G, Scargiali F, et al. Thermolytic reverse electrodialysis heat engine: model development, integration and performance analysis. Energy Convers Manag 2019;189:1–13.
[18] Lin S, Yip NY, Elimelech M. Direct contact membrane distillation with heat recovery: thermodynamic insights from module scale modeling. J Membr Sci 2014;453:498–515.
[19] Kuang Z, Long R, Liu Z, Liu W. Analysis of temperature and concentration polarizations for performance improvement in direct contact membrane distillation. Int J Heat Mass Tran 2019;145:118724.
[20] Achilli A, Childress AE. Pressure retarded osmosis: from the vision of Sidney Loeb to the first prototype installation — Review. Desalination 2010;261(3):205–11.
[21] Tedesco M, Cipollina A, Tamburini A, Bogle IDL, Micale G. A simulation tool for analysis and design of reverse electrodialysis using concentrated brines. Chem Eng Res Des 2015;93:441–56.
[22] Long R, Lai X, Liu Z, Liu W. A continuous concentration gradient flow electrical energy storage system based on reverse osmosis and pressure retarded osmosis. Energy 2018;152:896–905.
[23] Lacey RE. Energy by reverse electrodialysis. Ocean Eng 1980;7(1):1–47.
[24] Ramon GZ, Feinberg BJ, Hoek EMV. Membrane-based production of salinity-gradient power. Energy Environ Sci 2011;4(11):4423–34.
[25] Long R, Li B, Liu Z, Liu W. Reverse electrodialysis: modelling and performance analysis based on multi-objective optimization. Energy 2018;151:1–10.
[26] Long R, Li B, Liu Z, Liu W. Performance analysis of reverse electrodialysis stacks: channel geometry and flow rate optimization. Energy 2018;158:427–36.
[27] Long R, Kuang Z, Liu Z, Liu W. Reverse electrodialysis in bilayer nanochannels: salinity gradient-driven power generation. Phys Chem Chem Phys 2018;20:7295–302.
[28] Long R, Kuang Z, Liu Z, Liu W. Ionic thermal up-diffusion in nanofluidic salinity-gradient energy harvesting. Natl Sci Rev 2019;6(6):1266–73.
[29] Long R, Luo Z, Kuang Z, Liu Z, Liu W. Effects of heat transfer and the membrane thermal conductivity on the thermally nanofluidic salinity gradient energy conversion. Nanomater Energy 2020;67:104284.
[30] Mei Y, Tang CY. Recent developments and future perspectives of reverse electrodialysis technology: a review. Desalination 2018;425:156–74.
[31] Kim DH, Park BH, Kwon K, Li L, Kim D. Modeling of power generation with thermolytic reverse electrodialysis for low-grade waste heat recovery. Appl Energy 2017;189:201–10.
[32] Long R, Li B, Liu Z, Liu W. Hybrid membrane distillation-reverse electrodialysis electricity generation system to harvest low-grade thermal energy. J Membr Sci 2017;525:107–15.
[33] Tufa Ramato A, Curcio E, Brauns E, van Baak W, Fontananova E, Di Profio G. Membrane distillation and reverse electrodialysis for near-zero liquid discharge and low energy seawater desalination. J Membr Sci 2015;496:325–33.
[34] Ghaffour N, Soukane S, Lee JG, Kim Y, Alpatova A. Membrane distillation hybrids for water production and energy efficiency enhancement: a critical review. Appl Energy 2019;254:113698.
[35] Lee J-G, Kim Y-D, Shim S-M, Im B-G, Kim W-S. Numerical study of a hybrid multi-stage vacuum membrane distillation and pressure-retarded osmosis system. Desalination 2015;363:82–91.
[36] Brogioli D, La Mantia F, Yip NY. Energy efficiency analysis of distillation for thermally regenerative salinity gradient power technologies. Renew Energy 2019;133:1034–45.
[37] Yip NY, Brogioli D, Hamelers HVM, Nijmeijer K. Salinity gradients for sustainable energy: primer, progress, and prospects. Environ Sci Technol 2016;50(22):12072–94.
[38] Jiang L, Wang L, Wang R, Gao P, Song F. Investigation on cascading cogeneration system of ORC (Organic Rankine Cycle) and CaCl2/BaCl2 two-stage adsorption freezer. Energy 2014;71:377–87.
[39] Zhang N, Lior N. Development of a novel combined absorption cycle for power generation and refrigeration. Journal of Energy Resources Technology-transactions of The Asme - J ENERG RESOUR TECHNOL 2007;129.
[40] Al-Mousawi FN, Al-Dadah R, Mahmoud S. Low grade heat driven adsorption system for cooling and power generation with small-scale radial inflow turbine. Appl Energy 2016;183:1302–16.
[41] Olkis C, Santori G, Brandani S. An Adsorption Reverse Electrodialysis system for the generation of electricity from low-grade heat. Appl Energy 2018;231:222–34.
[42] Pitzer KS, Mayorga G. Thermodynamics of electrolytes. II. Activity and osmotic coefficients for strong electrolytes with one or both ions univalent. J Phys Chem 1973;77(19):2300–8.
[43] Silvester LF, Pitzer KS. Thermodynamics of electrolytes. 8. High-temperature properties, including enthalpy and heat capacity, with application to sodium chloride. J Phys Chem 1977;81(19):1822–8.
[44] Dubinin MM, Astakhov VA. Development of the concepts of volume filling of micropores in the adsorption of gases and vapors by microporous adsorbents. Bulletin of the Academy of Sciences of the USSR, Division of chemical science 1971;20(1):8–12.
[45] Ramirez D, Qi S, Rood MJ, Hay KJ. Equilibrium and heat of adsorption for organic vapors and activated carbons. Environ Sci Technol 2005;39(15):5864–71.
[46] Wu JW, Hu EJ, Biggs MJ. Thermodynamic cycles of adsorption desalination system. Appl Energy 2012;90(1):316–22.
[47] Long R, Zhao Y, Luo Z, Li L, Liu Z, Liu W. Alternative thermal regenerative osmotic heat engines for low-grade heat harvesting. Energy 2020;195:117042.
[48] Lange MFd, BLv Velzen, Ottevanger CP, Verouden KJFM, Lin L-C, Vlugt TJH, et al. Metal–organic frameworks in adsorption-driven heat pumps: the potential of alcohols as working fluids. Langmuir 2015;31(46):12783–96.
[49] Zafarani-Moattar MT, Nasirzade K. Osmotic coefficient of methanol + LiCl, + LiBr, and + LiCH3COO at 25 °C. J Chem Eng Data 1998;43(2):215–9.
[50] Sardroodi JJ, Seyed Ahmadian SM, Pazuki GR, Sadr Moayad H, Esmaili M. Osmotic and activity coefficients in the solutions of 1- and 2-naphthol in methanol and ethanol at 298.15 K. Calphad 2006;30(3):326–33.
[51] Zafarani-Moattar MT, Aria M. Isopiestic determination of osmotic and activity coefficients for solutions of LiCl, LiBr, and LiNO3 in 2-propanol at 25°C. J Solut Chem 2001;30(4):351–63.
[52] Dunn LA, Stokes RH. Pressure and temperature dependence of the electrical permittivities of formamide and water. Trans Faraday Soc 1969;65:2906–12.0.
[53] Bezman RD, Casassa EF, Kay RL. The temperature dependence of the dielectric constants of alkanols. J Mol Liq 1997;73–74:397–402.
[54] Paschek D. Temperature dependence of the hydrophobic hydration and interaction of simple solutes: an examination of five popular water models. J Chem Phys 2004;120(14):6674–90.
[55] Haghbakhsh R, Raeissi S. Densities and volumetric properties of (choline chloride + urea) deep eutectic solvent and methanol mixtures in the temperature range of 293.15–323.15 K. J Chem Therm 2018;124:10–20.
[56] Jing H, Exell RHB. Adsorptive properties of activated charcoal/methanol combinations. Renew Energy 1993;3(6):567–75.
[57] El-Sharkawy II, Hassan M, Saha BB, Koyama S, Nasr MM. Study on adsorption of methanol onto carbon based adsorbents. Int J Refrig 2009;32(7):1579–86.
[58] Wu JW, Madani SH, Biggs MJ, Phillip P, Lei C, Hu EJ. Characterizations of activated carbon-methanol adsorption pair including the heat of adsorptions. J Chem Eng Data 2015;60(6):1727–31.
[59] Passos E, Meunier F, Gianola JC. Thermodynamic performance improvement of an intermittent solar-powered refrigeration cycle using adsorption of methanol on activated carbon. J Heat Recovery Syst 1986;6(3):259–64.
[60] Henninger SK, Schicktanz M, Hügenell PPC, Sievers H, Henning HM. Evaluation of methanol adsorption on activated carbons for thermally driven chillers part I: thermophysical characterisation. Int J Refrig 2012;35(3):543–53.
[61] Hamamoto Y, Alam KCA, Saha BB, Koyama S, Akisawa A, Kashiwagi T. Study on adsorption refrigeration cycle utilizing activated carbon fibers. Part 1. Adsorption characteristics. Int J Refrig 2006;29(2):305–14.
[62] De Lange MF, Van Velzen BL, Ottevanger CP, Verouden KJFM, Lin LC, Vlugt TJH, et al. Metal-organic frameworks in adsorption-driven heat pumps: the potential of alcohols as working fluids. Langmuir 2015;31(46):12783–96.
[63] de Lange MF, Verouden KJFM, Vlugt TJH, Gascon J, Kapteijn F. Adsorption-driven heat pumps: the potential of metal–organic frameworks. Chem Rev 2015;115(22):12205–50.